JBIC (2000) 5 : 16–19

MINIREVIEW

David W. Randall · Daniel R. Gamelin
Louis B. LaCroix · Edward I. Solomon

Electronic structure contributions to electron transfer in blue Cu and Cu_A

Received: 15 October 1999 / Accepted: 29 November 1999

Abstract The experimentally determined electronic structures of mononuclear blue Cu and binuclear Cu_A centers are summarized and their relation to intra- and inter-protein electron transfer (ET) kinetics are described. Specific contributions of the electronic structures of these two broad classes of Cu ET proteins to H_{AB}, λ, and ΔE° are discussed. Also, the role of the protein structure in determining key geometric features which define the electronic structures of the metal sites in these proteins is considered.

Key words Blue copper proteins · Electron transfer kinetics · Cu_A Center

Introduction

Rapidly transferring electrons within biological systems, while minimizing unwanted, potentially damaging redox reactions, is an extremely important process in living systems. The task of intra- and inter-protein electron transfer (ET) is admirably performed by copper-containing proteins, specifically the widely distributed mononuclear blue (type 1, T1) copper (Fig. 1A) [1–6] and binuclear purple Cu_A centers (Fig. 1B) [7–9]. A high rate of directional ET is key to the required specificity. The rate of biological ET is dependent upon three terms described in the semiclassical Marcus equation (Eq. 1) [10]: the donor-acceptor electronic coupling, H_{AB}; the vibronic or Franck-Condon reorganization energy associated with redox, λ; and the difference in reduction potentials between the electron acceptor and donor (i.e., the driving force of the ET reaction), ΔE°.

$$k_{ET} = \sqrt{\frac{\pi}{\hbar^2 \lambda k_B T}} (H_{AB})^2 \exp\left[-\frac{(\Delta E^\circ + \lambda)^2}{4\lambda k_B T}\right] \quad (1)$$

Here $k_B T$ is the thermal energy. This equation demonstrates that the ET rate will be enhanced by maximizing H_{AB} while minimizing the sum $\Delta E^\circ + \lambda$. In this paper we evaluate the specific contribution to each of these three terms from the experimentally defined electronic structural properties of both mononuclear (blue Cu) and binuclear (Cu_A) ET sites. We further use experimental results to consider how the protein environment influences the geometrical and electronic structures of these Cu centers and thus can affect the ET function.

Mononuclear blue copper

Blue Cu proteins use the Cu(I/II) redox couple for ET. However, the reduction potential for blue Cu centers is higher (180–780 mV) than in an aqueous environment (~150 mV) [5, 6]. The Cu site in such classic blue Cu proteins as plastocyanin [11] (Fig. 1A) and azurin [12, 13] exhibits an elongated approximately C_{3v} trigonally distorted tetrahedral geometry with a ligand set in which two histidine (His) N^δ atoms with typical Cu-N bonds (~2.0 Å) and a cysteine (Cys) S^γ with an unusually short Cu-S bond (~2.1 Å) form an approximately trigonal plane to which the Cu atom is closest (Fig. 1A). A weak axial ligand completes the site; most often it is a methionine (Met) S^δ exhibiting a long, ~2.8 Å, Cu-S bond. A very long ~3 Å Cu-O bond to a backbone amide carbonyl oxygen, *trans* to the thioether, is sometimes discussed for azurin; however, at this distance, little covalent bonding interaction is present between the Cu and the compact O 2p orbitals [14].

D.W. Randall · D.R. Gamelin · L.B. LaCroix
E.I. Solomon (✉)
Department of Chemistry, Stanford University, Stanford, CA 94305, USA
e-mail: edward.solomon@stanford.edu
Fax: +1-650-7250259

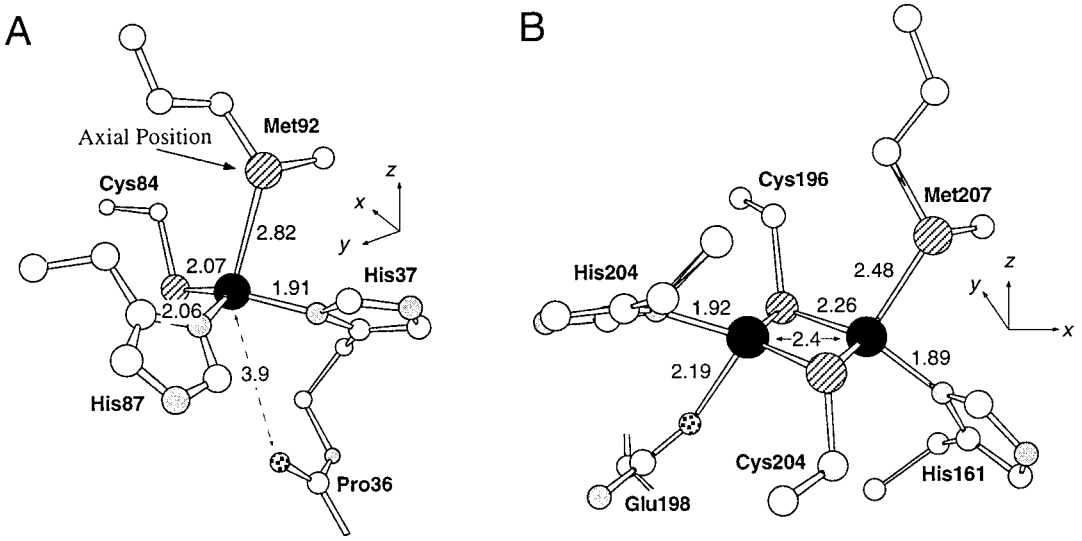

Fig. 1A,B The structures of Cu ET proteins. **A** The monomeric blue Cu center (pdb 1plc) [11]. **B** The binuclear Cu_A site (pdb 1occ) [86, 87]

H_{AB} in blue copper

Perhaps the most striking features of oxidized blue Cu proteins are an intense absorption band at ~600 nm ($\varepsilon \approx 5000\ cm^{-1}\ M^{-1}$) and a small Cu $A_{\|}$ value ($A_{\|} \leq 100\times10^{-4}\ cm^{-1}$) in the EPR spectrum [1–6, 15]. We have shown that these unique spectral features, originally ascribed to either covalency [16] or $4p_z$ mixing [17–20], in fact reflect a highly covalent electronic structure from the thiolate S_{Cys}-Cu π bond which is crucial to the center's function [15]. A direct experimental measure of the covalency of the blue Cu site has been made with S K-edge X-ray absorption spectroscopy (XAS) [21]. Since the S character in the half-occupied HOMO involves the S 3p orbitals and the 1s→3p transition is electric dipole allowed, the intensity of the S XAS pre-edge feature (i.e., the S 1s→HOMO transition) in the S K-edge XAS spectrum will be quantitatively related to the S covalency in the redox-active HOMO. Figure 2A compares the S K-edge XAS absorption of plastocyanin with that of a model complex (tet b) [22] with a normal Cu(II)-thiolate bond. The results of this experiment (Fig. 2A) demonstrate a highly covalent site in the blue Cu protein plastocyanin with ~38% S covalency [21]. Complementary Cu L edge XAS experiments [23], which quantitate the metal d character in the HOMO, reveal a low (42%) Cu contribution relative to normal Cu complexes, again demonstrating that the blue Cu center is highly covalent. EPR experiments on plastocyanin had revealed Cu $d x^2-y^2$ character in the HOMO that single crystal EPR measurements show to be oriented approximately in the $(N_{His})_2S_{Cys}$ plane [i.e., the electronic z axis is approximately along the long thioether S_{Met}-Cu(II) bond] [24]. Therefore, the $d x^2-y^2$ orbital is oriented such that S_{Met} makes very little contribution to the HOMO. Consequently, the high experimental S covalency in plastocyanin derives from an extremely covalent Cu-S_{Cys} thiolate interaction [15].

The presence of the intense low-energy ~600 nm absorption band gave additional insight into the electronic structure [5, 6, 15]. From a combination of low-temperature absorption and magnetic circular dichro-

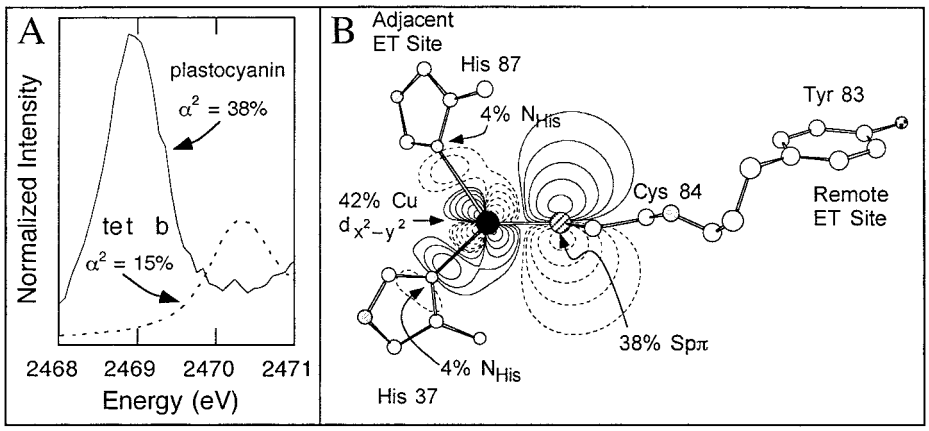

Fig. 2A,B H_{AB} in blue copper. **A** S K-edge experiments [21] show a ~38% sulfur covalency relative to ~15% in the tet-b model complex which exhibits a "normal" Cu-S (thiolate) bond length of ~2.36 Å [22]. **B** A contour of the plastocyanin HOMO showing the large anisotropic covalency of the Cu-S_{Cys} π-type antibonding interaction which facilitates ET to the remote site

ism (MCD) spectroscopies this band could be assigned as the lowest energy $S_{Cys}\pi \rightarrow$ Cu $d x^2-y^2$ charge transfer (CT) transition, while the higher energy $S_{Cys}\sigma \rightarrow$ Cu $d x^2-y^2$ has a very low absorption intensity. In typical (tetragonal) Cu(II) centers the lowest energy π CT band has little intensity and the higher energy σ CT band is more intense. This π/σ CT spectral intensity pattern reveals that in blue copper there is a large overlap between the S_{Cys} p π orbital [this orbital is oriented perpendicular to the Cu-S_{Cys} bond, but in the $(N_{His})_2S_{Cys}$ plane] and the HOMO orbital which gives this CT transition considerable intensity, while the lower intensity of the higher energy CT band involving the S_{Cys} p pseudo-σ orbital (roughly colinear with the Cu-S_{Cys} bond) indicates reduced orbital overlap with the HOMO [15]. Thus, the Cu-S_{Cys} CT band intensities quantitate the nature of the Cu-S_{Cys} bonding interactions and hence the orientation of the $d x^2-y^2$ orbital in the $(N_{His})_2S_{Cys}$ plane (Fig. 2B).

To add a theoretical dimension to our experimental picture of the electronic structure in the prototypical plastocyanin blue Cu site, self-consistent field-Xα-scattered wave (SCF-Xα-SW) calculations [25, 26] were performed [27–29]. These calculations were adjusted to experiment by varying the atomic sphere radii used in the SW solutions such that the experimental EPR *g*-values were reproduced [27, 28]. The resulting calculated wavefunction was found to reproduce key experimentally derived properties of the blue Cu HOMO, including the orientation, large S_{Cys} covalency, small N_{His} covalency [30], and $d x^2-y^2$ Cu character. Further, these Xα-SW calculations from over a decade ago [27] showed a Cu-S_{Cys} π anti-bonding interaction in the HOMO (Fig. 2B), consistent with the intense, low-energy CT transition observed in electronic absorption spectroscopy. Recent calculations [31, 32] using different computational methods also show this interaction. We emphasize that while calculations can provide complementary insight, the key features of the blue Cu site, including high covalency, orientation of the redox active orbital, and other factors (vide infra), have been derived from experiment.

Blue Cu proteins such as plastocyanin, nitrite reductase, ascorbate oxidase, etc. use two sites for ET (Fig. 2B) [5, 6]. The remote site is ~13 Å from the blue Cu center and the most likely pathway to it involves significantly more covalent bonds through the protein than that to the adjacent site, which is only ~5 Å from the Cu ion. The through-bond pathway to the remote site goes through the S_{Cys} of the blue copper site to an adjacent residue in the primary amino acid sequence which is at the remote ET site[1]. The Cys-Tyr ET pathway to the remote site in plastocyanin contains 11 covalent bonds (in ascorbate oxidase [33] and nitrite reductase [34] the analogous Cys-His pathway to the type 3/type 2 cluster or the T2 copper, respectively, contains 9 covalent bonds). On the other hand, the adjacent ET site involves one of the Cu-ligated N_{His} sidechains, which is on the surface of the protein, and involves two covalent bonds. For plastocyanin, the ET rates to both sites are found to be similar despite the large difference in the lengths of ET paths [35]. This is attributed to differences in the degree of covalent coupling into the two pathways which affects the electronic coupling, H_{AB}. The ET rate to the distant site is facilitated by the large Cu-S_{Cys} covalency, which greatly enhances H_{AB} along this ~8 Å longer S_{Cys} pathway (Fig. 2B) [36]. Since H_{AB} affects the ET rate quadratically, the ~10-fold greater covalency of S_{Cys} over N_{His} (the covalency of each N_{His} is about 4%, from both ENDOR studies [30] and calculations [27–32]) makes the ET rate equivalent to a pathway with ~9 fewer covalent bonds (using a decay factor of 0.6 per bond [37]). In multicopper proteins (i.e., nitrite reductase and multicopper oxidases) it seems clear that an electron enters the blue Cu site through the His and leaves the blue site via a Cys-His pathway to the enzymatically active type 2 or type 3/type 2 Cu cluster[2]. Thus, the experimentally determined anisotropic covalency of the redox active orbital in the blue Cu site is important to the intra- and inter-protein long-range ET function through its effect on H_{AB} in Eq. 1 [36].

E° in blue copper

Experimentally evaluating the electronic structure contribution to the ET rate involves studying the reduced blue Cu site and therefore probing the d^{10} configuration. This full d subshell makes it inaccessible to the usual array of bioinorganic spectroscopic techniques. To better define this site and its change upon oxidation, we have used variable-energy photoelectron spectroscopy (PES) for Cu(I) complexes where small-molecule ligands relevant to blue copper are bound to coordinatively unsaturated Cu(I) sites on oxide and chloride single-crystal surfaces in ultra-high vacuum [38–40]. Such model complexes, rather than proteins, are studied since we want to understand normal ligand-and-metal bonding in relation to bonding in the reduced blue Cu center [41]. These experiments, then, define the geometric and electronic structure of an unconstrained ligand-Cu(I) bond. Calculations, experimentally calibrated with the PES data, generate an electronic structure description of the reduced blue copper site and permit evaluation of the change in electronic structure upon oxidation [41].

[1] Note that this is a hole superexchange pathway, as the high covalency of the thiolate-Cu(II) bond creates partial hole character in the occupied valence orbital of the protein pathway to the remote ET site

[2] In other mononuclear blue Cu proteins, such as azurin, the degree to which the remote site participates in ET appears to be uncertain

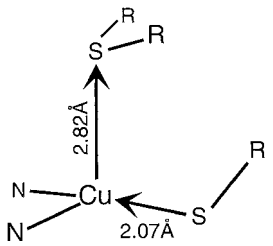

Fig. 3 Effects of the protein on ligand donor interactions of the blue copper active site. Arrows show decreased electron donation from S_{Met} (long thioether-Cu bond) and resulting increased electron donation from S_{Cys} (short thiolate-Cu bond). Together these minimize the tetragonal distortion (see Fig. 4)

This approach [41] has enabled us to determine that the bonding in the reduced blue copper site is dominated by ligand p donor interactions with the unoccupied Cu(I) 4s and 4p levels. There is no evidence for back-bonding. Additionally, the long S_{Met}-Cu(I) bond in the reduced blue Cu center does not appear to be present in the unconstrained surface complexes and does not derive from the electronic structure of the reduced blue copper site [41]. This elongated thioether bond reduces the donor interaction of this ligand with the reduced copper. This is compensated for by the thiolate, leading to the short, strong S_{Cys}-Cu(I) bond (Fig. 3) [15, 41]. The long thioether S_{Met}-Cu bond should reduce the donor interaction with the Cu(II) more than Cu(I), destabilizing the oxidized site more than the reduced site which would contribute to the high reduction potential of the blue copper center.

Many factors contribute to the high reduction potential of the blue Cu centers, including the protein environment (local dielectric, H-bonding, and carbonyl and water dipoles, etc.), ligation, and change in geometry with redox state ([42] and refs. therein; see also, for instance [43, 44][3]). This can be seen in the potentials of fungal laccases, where the oxidized blue copper sites are all spectroscopically equivalent, yet their potentials span a range of ~300 mV [52]. To experimentally evaluate the influence of the axial position on the reduction potential, a single mutation at this position minimizes these environmental factors and the results are summarized in Table 1. For wild-type *Polyporus pinsitus* fungal laccase, the T1 axial liganding position (the Met in plastocyanin) is occupied in the primary amino acid sequence by Phe, which does not ligate to the Cu [52, 53]. The reduction potential of this blue Cu center is 780 mV. Substitution of this Phe using site-directed mutagenesis with coordinating Met lowers the reduction potential by ~100 mV [54]. Similar experiments in the blue Cu protein azurin show that substitution of the axial Met ligand in the wild-type protein with bulky, non-ligating residues such as Leu, Ile, or Val raises the potential by ~100 mV [55][4]. Further, in the Az series, substitution of the Met with a stronger ligand lowers the potential by an amount which depends upon the nature of the axial ligand [55–57][5]. Wild-type stellacyanin has a stronger axial Gln ligand occupying the position typically occupied by Met and a low potential of 260 mV (cucumber stellacyanin) [58]. Replacement of this Gln with a weaker Met ligand raises the potential by 160 mV [58]. The related phytocyanin mavicyanin exhibits similar a change in $E°$ [59]. Further, for the perturbed blue Cu center (vide infra) in *Rhodobacter sphaeroides* nitrite reductase, mutating the axial Met to non-ligating Thr increases the reduction potential from 250 mV to 350 mV [60]. Thus, multiple experimental results in both a fixed protein environment and wild-type proteins (fungal laccase→plastocyanin→stellacyanin) reveal that as the strength of the axial ligand increases the potential decreases. This trend was also qualitatively observed in the results of Xα-SW calculations [41], which, however, significantly overestimate the magnitude of this effect relative to experiment. The high reduction potential of the blue copper center affects the ET rate by providing the thermodynamic driving force for rapid ET with its physiological partners.

Table 1 Dependence of E° on the axial ligand in Blue Cu mutant proteins

Blue Cu Protein	Axial Ligand			Ref
	Phe/Leu	Met	Gln	
Fungal Laccase	+770	+680	–	[52–54]
Azurin	+412	+310	+285	[55–57]
Cuc. Stellacyanin	–	+420	+260	[58]

λ in blue copper

For ET carriers relying on the Cu(I)/Cu(II) redox couple, such as blue Cu centers, minimizing the reorganization energy, λ in Eq. 1, is extremely important, since in the absence of a constraining ligand environment, significant geometrical changes (i.e., from tetrahedral to tetragonal) often accompany oxidation in Cu model

[3] Also, JBIC (1997) vol 2, no 1 has a commentary section dedicated to different factors influencing reduction potentials [45–51]

[4] The changes in the reduction potential with respect to wild-type protein are: Met→Leu, +102 mV, *Pseudomonas aeruginosa* Az [55]; Met→Ile, +138 mV *P.a.*Az [55]; Met→Val, +135 mV *P.a.*Az [55]

[5] The changes in the reduction potential with respect to wild-type protein are: Met→His, –75 mV, *Alcaligenes denitrificans* Az [56], 0 mV *P.a.*Az [55]; Met→Gln, –25 mV *A.d.*Az [57]; Met→End (axial H_2O), –105 mV *P.a.*Az [55]. The *P.a.*Az M121H mutant reduction potential may be influenced by the pH of the measurement. For the *A.d.*Az M121Q mutant, the geometry changes upon reduction to a more typical Cu(I) bonding motif [57]. The observed decrease in potential relative to wild-type is likely buffered by this geometry change

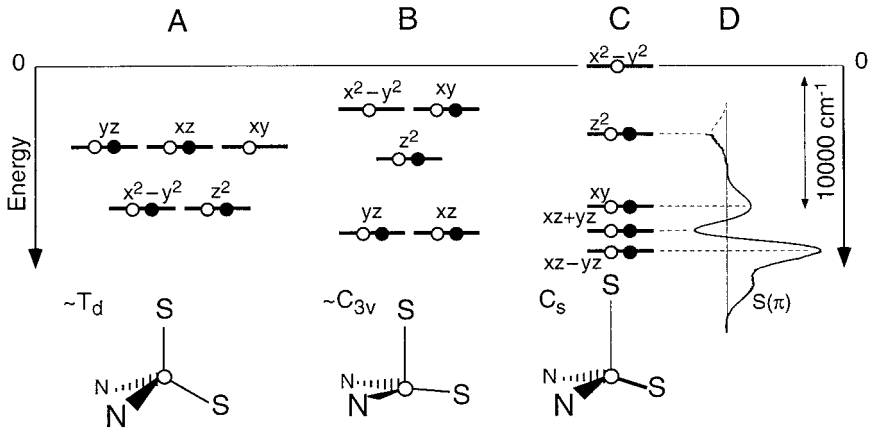

Fig. 4A–D Depiction of how the ligand field of a classic blue copper center minimizes λ. Energy level diagrams show that idealized **A** T_d (see footnote 8) and **B** C_{3v} (following introduction of long Cu-S_{Met} bond) are both subject to Jahn-Teller (JT) distortions upon oxidation, while the **C** C_s structure resulting from the associated contraction of the Cu-S_{Cys} bond is not. The LT-MCD spectrum [28, 29] of plastocyanin (**D**) experimentally measures the d orbital splitting (see footnote 7) and demonstrates that the dx^2–y^2 and dxy orbitals are split by over 10,000 cm^{-1}, eliminating the JT distorting forces of the oxidized site

systems [61, 62]. These large structural changes associated with redox state are due to a Jahn-Teller (JT) distorting force present in typical oxidized Cu (d^9) centers, leading to a tetragonal (i.e., square planar) geometry. This JT force is associated with partially unoccupied valence d orbital degeneracy.

From the above studies the change in electronic structure of the blue Cu center on oxidation involves the hole produced in the dx^2-y^2 orbital which is antibonding to the Cys thiolate and to the two His ligands (Fig. 2B). This change in electronic structure allows an estimate [41] of the new forces present upon oxidation which would distort the structure[6]. In oxidized blue Cu centers the JT force has been substantially diminished by the site's unique ligand geometry and its influence on the d-manifold orbital energy splittings, which can be experimentally measured with low-temperature MCD in the near-IR spectral region [15][7].

Figure 4 correlates the changes in the d-level splitting patterns with geometric distortions of the oxidized blue copper center from the idealized tetrahedral limit. The tetrahedral starting point (Fig. 4A, one hole in the three-fold degenerate dxy, dxz, dyz set[8]) would be subject to a large JT distortion. The C_{3v} distorted (elongated trigonal) structure (Fig. 4B, one hole in the two-fold degenerate dx^2-y^2 dxy set), which results from lengthening the axial thioether ligand, would be subject to a similar distortion. Shortening the thiolate bond to charge-compensate for the weakened axial thioether ligand results in C_s geometry for the blue Cu site, which finally eliminates all the JT orbital degeneracy in the oxidized site (Fig. 4C); this degeneracy could have resulted in a non-zero JT force in the tetrahedral and C_{3v} intermediate structures (Fig. 4A, B). The experimental d→d transitions observed in the MCD spectrum of plastocyanin (see footnote 7) (Fig. 4D) demonstrate that the shortened thiolate bond splits the dx^2-y^2 and dxy orbital energies by ~10,000 cm^{-1}. Thus, the elongated $C_{3v}\rightarrow C_s$ distorted tetrahedral geometry of the reduced blue Cu center generates a ligand field that removes the JT orbital degeneracy that typically determines the geometry of normal oxidized Cu centers. The reduced blue Cu protein environment, therefore, minimizes the inner-sphere reorganization energy (λ_{inner}) upon oxidation and the ET rate is enhanced relative to normal copper complexes.

Protein structure influences in blue copper

From early studies on the unique spectral features of blue copper centers it has been thought that the protein plays a role in the geometry of the site that affects its reactivity (λ and $E°$). This situation has been termed the entatic [61] or rack-induced [65] state. It has been generally thought that the reduced

[6] These were determined [41] by evaluating the electon-nuclear linear coupling terms of the oxidized site in the reduced geometry along the normal modes of the blue Cu site. The forces obtained are consistent with the limited geometric structural changes which are observed from crystallography [11, 63] upon oxidation: contraction of the thiolate S_{Cys}-Cu and two N_{His}-Cu bonds. No bending force was observed, consistent with the lack of significant angle changes of the blue Cu center upon oxidation. Therefore, there is no JT distorting force on the oxidized site

[7] It is important to note that MCD *C*-term intensity is determined by spin-orbit coupling. Therefore, d→d transitions, which are localized on the Cu center that has a large spin-orbit coupling constant (830 cm^{-1}), have very high intensity in the low-temperature MCD spectra. Alternatively, CT transitions involve the blue Cu ligands, where the highest spin-orbit coupling constant is that of sulfur (382 cm^{-1}), and their intensity is lower in the low-temperature MCD spectra [28]

[8] In the tetrahedral limit (Fig. 4A) the orbital labels use the improper four-fold axis as *z*. Upon trigonal elongation (Fig. 4B,C) the orbitals are labeled with the three-fold axis as *z* (see [64])

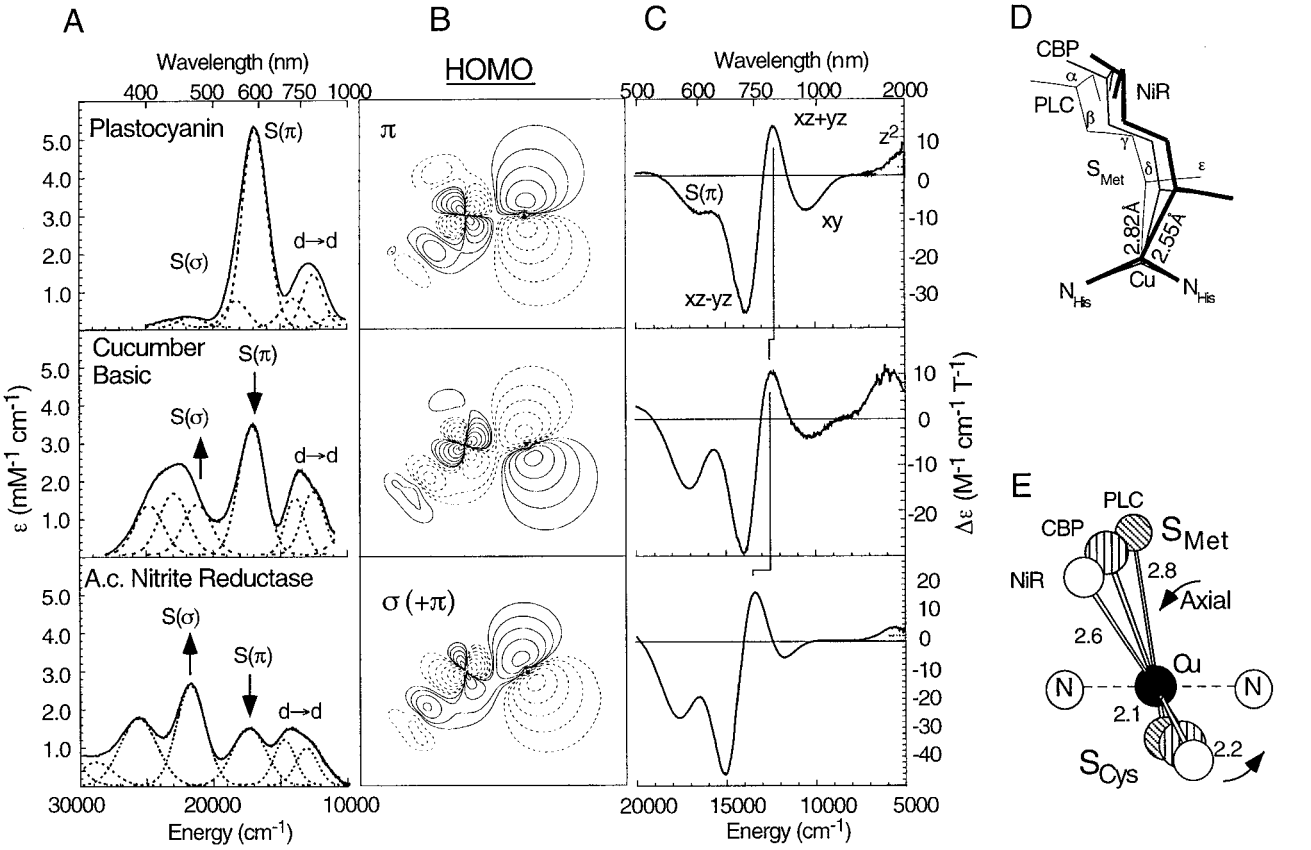

Fig. 5A–E Experimental evidence for an increasing tetragonal distortion in a series of blue copper proteins with the same ligand set. **A** Low-temperature absorption spectra [29, 67] show increasing intensity in the ~450 nm (Cys pseudo-σ CT) band at the expense of the ~600 nm (Cys π CT) band. **B** Half-occupied HOMOs perpendicular to the S_{Met}-Cu-S_{Cys} plane for plastocyanin, cucumber basic protein, and *A.c.*NiR calculated with Xα-SW [27–29, 67]. **C** The MCD spectra [29, 67] show an increase in d→d energy, consistent with a tetragonal (towards D_{4h}) distortion. The crystal structures [11, 34, 73] along with the data show that contraction of the S_{Met}-Cu bond (**D**) is associated with elongation of the S_{Cys}-Cu bond and a tetragonal distortion (**E**) in the ε(u) JT mode

structure was imposed on the oxidized site by the protein, which would raise its potential and lower the geometry change associated with redox state. In this model the protein would restrict the JT distortion of the oxidized site, which normally results in a tetragonal geometry for Cu(II) complexes. However, our studies have shown that there is no JT distorting force for the oxidized blue Cu site [15, 41]. Our studies have alternatively indicated that the 2.8 Å thioether S_{Met}-Cu(I) bond of the reduced site is longer than would be expected for a normal bond of this type[9], and as indicated above, the presence of this long bond is coupled to the formation of a short thiolate S_{Cys}-Cu(I) bond length which together eliminate the JT tetragonal distortion [41]. Thus, the Cu(II) site is not "energized" in the usual entatic sense of countering the JT distorting force. In our view, this coupled distortion (long thioether, short thiolate, and no tetragonal distortion) is imposed by the protein environment on the blue copper site of plastocyanin and azurin. The long thioether S_{Met}-Cu bond has reduced donor interactions with both the oxidized and reduced sites. This destabilizes the oxidized site more than the reduced site and results in an increase in the reduction potential.

This model for the protein's effect on the blue Cu site geometric and electronic structure can be evaluated in a series of blue Cu proteins which all have the same ligand set [29, 67] but yet exhibit perturbed spectral features relative to those of blue Cu centers like plastocyanin. By perturbed we mean that in the absorption spectra the intensity of the ~450 nm band increases with respect to that of the ~600 nm band, which can be expressed quantitatively as $R_\varepsilon = \varepsilon_{450}/\varepsilon_{600}$ [68], and the EPR spectra of perturbed blue Cu centers are more rhombic than plastocyanin. The series of proteins plastocyanin, cucumber basic protein (CBP, also called plantacyanin), and *Achromobacter cycloclastes* nitrite reductase (*A.c.*NiR) exhibit increasing R_ε values (see arrows in Fig. 5A) and rhombic EPR spectra [69, 70], yet they all have the same S_{Cys},

[9] A search of the CCDB for Cu(I)-SC_2 thioether bond distances (61 structures with $R \leq 10\%$) gives an average distance of 2.32 Å with a standard deviation of 0.066 Å. These were mostly four-coordinate complexes with N_2S_2 or S_4 ligand sets. The longest bond (2.6 Å) involves a bridging thioether between two approximately trigonal Cu(I) atoms [66]

S_{Met}, $2N_{His}$ ligand set. In CBP and *A.c.*NiR the ~450 nm band corresponds to an S p pseudo-$\sigma \rightarrow$HOMO CT absorption [29, 68, 71], while in all three the ~600 nm band corresponds to a S p $\pi \rightarrow$HOMO CT absorption (vide supra) [27, 28]. Since absorption intensity is proportional to orbital overlap, the increasing R_ε values across the series experimentally demonstrate the rotation of the HOMO from a pure π-type Cu-S_{Cys} interaction in plastocyanin to an S π/S pseudo-σ mixture with increasing amounts of S p pseudo-σ character along the series [67]. Even in the perturbed center in *A.c.*NiR, which is, at present, the limiting case of a perturbed blue Cu site, the substantial intensity of the ~600 nm absorption ($\varepsilon \approx 2000$ M^{-1} cm^{-1}) demonstrates that its HOMO still has some π character [29]. The shift to higher energy of the experimental d$\rightarrow$d energies measured by MCD (Fig. 5C) (see footnote 7) over this series shows that a tetragonal (not tetrahedral [72]) distortion occurs in these perturbed sites [29][10], which can be observed from crystallography (Fig. 5D, E) [11, 34, 73].

These electronic structural effects are linked to geometric perturbations relative to plastocyanin in this series of "blue" Cu proteins (*A.c.*NiR is actually green) [29]. X-ray crystallography [11, 34, 73] shows the axial S_{Met} interaction increases in strength in this series (the Cu-S_{Met} distance decreases), while the strength of the Cu-S_{Cys} bond decreases, as evidenced by crystallography [11, 34, 73] and the decrease in Raman stretching frequency ([74] and refs. therein). In the absence of other changes, the stronger axial ligand would generate a hypothetical more tetrahedrally distorted intermediate site (i.e., dx^2-y^2 and dxy closer in energy as in Fig. 4). This would increase the magnitude of the JT distorting force along an ε(u) mode, which is in fact observed experimentally (Fig. 5E) [29, 67]. This distortion is characterized by a rotation of the dihedral angle between the N_{His}-Cu-N_{His} and S_{Cys}-Cu-S_{Met} planes towards a tetragonal geometry (Fig. 5E) [29].

Thus, a coupled distortion is present in the site structures in Fig. 5 where the S_{Met}-Cu bond length decreases, the thiolate S_{Cys}-Cu bond length increases, and the site becomes more tetragonal. Since the ligand set is the same in all these sites, these differences must be imposed by the protein. The spectra and structures in Fig. 5 reflect a continuum of active site geometries and electronic structures [67], which reflect an entatic or rack-induced state for blue copper. By this we mean that the protein influences the active site geometric and electronic structure in a way that can affect reactivity. This differs from the proposal of Ryde et al. [75] who have argued, based on total energy density functional theory (DFT) calculations of the blue copper ligand set in vacuum, that the protein plays a minimal role in active site structure. Their later calculations [76] revise the proposal to deal with the spectral continuum [67]. They find two minima [76, 77] and suggest that the experimentally observed spectral changes arise from either an equilibrium mixture of trigonal and tetragonal limiting structures or a real geometric continuum, though no intermediate structures are found in their calculations. However, the presence of a single set of d$\rightarrow$d bands in the ~5 K spectra across the series [67] makes it clear that this is a continuum of geometries along the coupled distortion coordinate, rather than an equilibrium mixture of two limiting extremes [76]. Further, the strength of the axial ligand must play a role in determining the blue copper structure [15, 29, 41, 67] because, for example, elimination of the shorter thioether bond in nitrite reductase changes the site from a tetragonally perturbed green to a blue copper center with spectral features similar to plastocyanin [60].

In summary, the long thioether S_{Met}-Cu bond is coupled to the short thiolate S_{Cys}-Cu bond, which together eliminate the tetragonal JT distortion of the oxidized blue Cu. The protein determines the position of the blue Cu ligand set along this coupled distortion coordinate. A key component of this coordinate is the donor strength of the axial ligand, which can be modulated by a change in bond length or the nature of the axial ligand. A separate question is that of quantitation: how strongly are the redox properties of the site affected by the geometric and electronic structural changes in Fig. 5? The present data are limited here and are complicated by the fact that the different protein environments will change the dielectric at the site and other factors which will also significantly contribute to E° and k_{ET}. Our research now focuses on evaluating the geometric and electronic structures of tetragonally perturbed (i.e., strong axial) and classic (i.e., weak axial) blue copper centers in the same protein environment and how these correlate to ET properties. In passing, we note that experimental evidence suggests that the situation is modified in stellacyanin [67]. From significant decreases in the MCD-observed ligand field transition energies (rather than the calculated *i*ncreases in d$\rightarrow$d transition energies [78]), stellacyanin appears to represent a separate class of perturbed blue copper centers. The axial S_{Met} ligand is replaced with an O_{Gln}, a stronger axial ligand that shifts the Cu out of the $S_{Cys}(N_{His})_2$ plane, to provide a more tetrahedral site [67].

Binuclear Cu_A

The valence delocalized, binuclear [79, 80] Cu_A center uses the Cu(1.5,1.5)/Cu(I,I) couple for inter- and intraprotein ET in nitrous oxide reductase and cytochrome oxidase. In cytochrome *c* oxidase (C*c*O), electrons enter the Cu_A center from cytochrome *c*. From Cu_A they are passed to the heme *a* center and subsequently

[10] A tetrahedral distortion would decrease the energy of the d$\rightarrow$d bands in the MCD spectrum

to the heme a_3/Cu_B center where oxygen is reduced to water [81, 82]. This produces a transmembrane proton gradient used to generate ATP [7, 8, 83]. Crystal structures of subunit II, whose only metal center is Cu_A, from three organisms [84–88], a loop-directed mutant in Az [89], and EXAFS data [90, 91] indicate that the Cu_A center contains a planar $Cu_2(S_{Cys})_2$ core (using S^γ of Cys-196-II and Cys-200-II[11]) with a ~2.44 Å Cu-Cu distance in the oxidized form and a 2.52 Å distance in the reduced form (for *Thermus thermophilus*; distances similar for other Cu_A centers) [90] (Fig. 1B). The Cu atoms are also ligated with short Cu-N_{His} bonds (~1.9 Å, from N^δ of His-161-II and His-204-II) which are roughly (but not exactly) parallel to the Cu-Cu axis and slightly removed from the plane [93]. The axial liganding position is occupied by an S_{Met} (from Met-207-II) on one Cu and a backbone peptide oxygen (from Glu-198-II) on the second. Like the Cys sidechains, the axial ligands occur on opposite sides of the $Cu_2(S_{Cys})_2$ plane. Our studies on Cu_A [94] have focused on understanding its electronic structure and the contribution to reactivity, the interactions between the coppers leading to electron delocalization, and the contribution of the ligand field to this delocalization. A key component of these studies has been a correlation to the electronic structure of the mixed valence [MV, Cu(1.5,1.5)] model compound prepared by Tolman and co-workers [95] which also has a $Cu_2(SR)_2$ core, but with a 2.9 Å Cu-Cu distance[12].

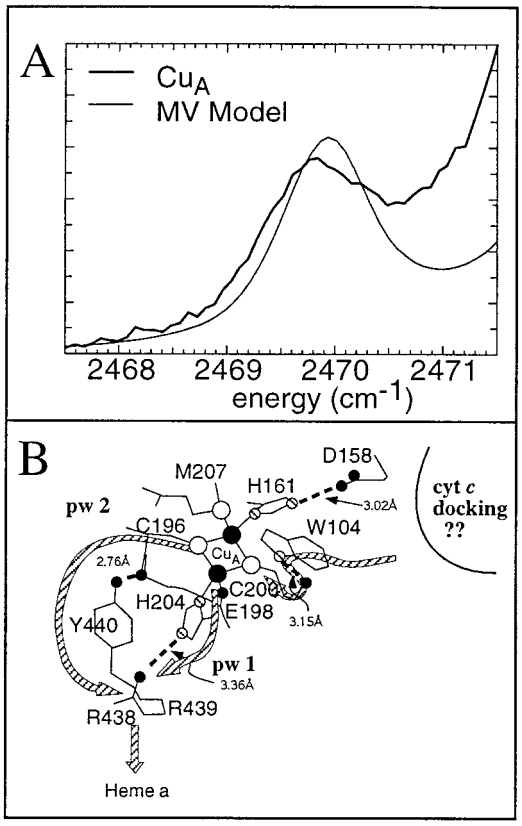

Fig. 6A,B H_{AB} in Cu_A. **A** S K-edge XAS experiments show that Cu_A has a similar covalency to that of the MV model. **B** Possible ET pathways into and out of the Cu_A center

H_{AB} in Cu_A

S K-edge XAS experiments (Fig. 6A) indicate that the Cu_A site is very covalent[13] and that the covalency is very similar to that of the MV model complex ([99], S. DeBeer, D. W. Randall, Y. Lu, W. B. Tolman, B. Hedman, K. O. Hodgson, E. I. Solomon, unpublished results). As in the blue Cu center [36], the high S covalency in the HOMO biases ET pathways both to and from Cu_A that involve S_{Cys} ligands [94, 99]. The S covalency of the Cu_A site makes a Cys-196-II based pathway from Cu_A to heme *a* (Fig. 6B) [94, 99] approximately competitive with the more direct His-204-II pathway (Fig. 6B) [8], though the importance of this pathway still needs to be experimentally quantitated. While the specifics of ET from Cu_A to heme *a* have received much attention [8, 82, 94, 99], the intermolecular ET process between cytochrome *c* and Cu_A is also important to consider, because unlike the blue Cu centers the Cu_A center in C*c*O does not have a surface-accessible ligating residue. Thus, protein-based ET pathways into Cu_A are functionally relevant. Recent mutagenesis experiments suggest that Trp-104-II is a key residue in the ET pathway from the cytochrome *c* docking site to Cu_A [102]. The indole ring of this Trp is on the cytosol-exposed surface. A reasonable electron input pathway to Cu_A proceeds through this residue, across an H-bond, and then through a Cu_A-ligating Cys (Cys-200-II) to the Cu_A core (Fig. 6B), for which the high S covalency (i.e., H_{AB}) of the Cu_A site can significantly enhance the Cu_A input ET rate.

ΔE° in Cu_A

In Cu_A, the strong covalent thiolate donor interactions are expected to stabilize oxidized Cu(II) while the long axial donor ligand would tend to destabilize the oxidized more than the reduced site [94]. In blue Cu these effects, combined with the protein environment, place the reduction potential in the physiologically necessary range. In Cu_A, however, the two covalent S_{Cys} ligands would significantly stabilize an oxidized Cu center such that it might be anticipated to have a

[11] Beef heart numbering; -II designates that the residue is in subunit II. See [7] and [92] for a useful table relating residue numbers in cyt *c* oxidase from common sources

[12] Other valence delocalized Cu dimers without bridging thiolates have been reported [96–98]

[13] The preliminary estimate of the covalency (26% total S character) [99] is in fact an underestimate (S. DeBeer, D. W. Randall, Y. Lu, W. B. Tolman, B. Hedman, K. O. Hodgson, E. I. Solomon, unpublished results) and the quantitization is consistent with the higher covalency from EPR studies [100, 101]

low reduction potential, below the observed value of +250 mV (vs. NHE) [103–106]. However, relative to a mononuclear Cu ion, the presence of a second copper ion and a strong interaction between the copper ions would tend to increase the effective nuclear charge (Z_{eff}) felt by the redox active electron (e.g., $[Cu(SR)_2]^0$ vs. $[Cu_2(SR)_2]^+$). An increase in Z_{eff} would increase the reduction potential of the Cu_A center. Thus, one of the major functional roles of the large metal-metal interaction in oxidized Cu_A (vide infra) may be to shift the reduction potential of a Cu center containing two thiolates into a range to react with its redox partners and minimize ΔE°.

λ in Cu_A

The valence delocalized, binuclear structure of Cu_A reduces its reorganization energy relative to blue Cu centers. An excited-state distortion analysis of the resonance Raman enhancement profile for Cu_A gives a value of $\sim 2000\ cm^{-1}$ for its inner-sphere reorganization energy for ET [94] compared to $\sim 3900\ cm^{-1}$ (using a similar analysis) for blue Cu [107]. Equation 2 provides an estimate [31, 108, 109] of the contribution to the inner-sphere reorganization energy from distortions associated with redox:

$$\lambda_{inner} \approx \frac{1}{2} k_{dis} n (\Delta r)^2 \qquad (2)$$

Here k_{dis} is the distortion force constant, n is the number of distorting metal-ligand bonds, and Δr is the magnitude of the change in the bond length with change in redox state. In evaluating the contribution of Δr to λ, we first compare a trapped valence or mononuclear center (case 1) to a valence delocalized Cu(1.5, 1.5) center (case 2). The latter has twice as many bonds changing (i.e., $n_2/n_1 = 2$), though the magnitude of their change will be approximately half as large (i.e., $\Delta r_2/\Delta r_1 = 1/2$). From Eq. 2 the inner-sphere reorganization energy contribution due to bond length distortions for the valence delocalized Cu_A center is reduced by a factor of ~one-half relative to either a mononuclear or trapped valence binuclear center [94, 110, 111]. The larger value of ν(Cu-S) for blue Cu complexes ($\sim 400\ cm^{-1}$) [72] relative to Cu_A ($\sim 270\ cm^{-1}$) [93, 112] reflects a lower value of k_{dis} in the latter, which further decreases the reorganization energy of Cu_A relative to the mononuclear Cu-thiolate center for metal-ligand bond length changes. There is, however, an additional distortion also possible in a dimer such as Cu_A that can make a contribution to λ_{inner}; this involves an in-plane bending distortion ($\Delta\theta$) of the Cu_2S_2 core (i.e., elongation along the Cu-Cu vector). Excited-state distortion [94] and EXAFS [90] measurements reveal that the distortion in this mode is significant (the change in the Cu-Cu distance is ≈ 0.1 Å [90]) and would therefore make an additional contribution to the inner-sphere reorganization energy. However, only a small amount of reorganization energy [$E_\lambda = (\Delta^2/2)\nu \approx 750\ cm^{-1}$, where the dimensionless parameter Δ is proportional to the displacement in the mode, i.e., $\Delta = \sqrt{k/\nu}\ (\Delta\theta)$] is associated with the binuclear core distorting mode, as this involves bends and a weak Cu-Cu stretch which has a low frequency ($\nu \approx 130\ cm^{-1}$ [93, 112]) [94]. Finally, the outer-sphere reorganization energy is also reduced by a valence delocalized binuclear center: studies [113] show an increase in ET rate with increasing electron donor charge radius (due to decreased solvent reorganization), such as found in the covalent, valence delocalized Cu_A core.

Presence of a Cu-Cu bond and its contribution to k_{ET}

Maintaining a valence delocalized Cu_2S_2 center, which enhances ET activity (vide supra), in the asymmetric Cu_A protein environment requires a strong Cu-Cu bonding interaction in the oxidized site (vide infra). The short Cu-Cu distance, in fact, allows for the possibility of a direct metal-metal bond in oxidized Cu_A [91]. The presence of a Cu-Cu bond in the oxidized electronic structure is experimentally verified through the increase in the energy of the dimer $\psi \rightarrow \psi^*$ transition[14] ($= 2H_{Cu\text{-}Cu}$, the electronic coupling between the Cu atoms [114, 115]) from $\sim 5600\ cm^{-1}$ in the MV model compound, where the 2.9 Å Cu-Cu distance precludes direct Cu-Cu bonding, to $\sim 13{,}400\ cm^{-1}$ in Cu_A (Fig. 7A) [94, 99]. The value of $2H_{Cu\text{-}Cu}$ is determined by contributions from metal-metal (direct exchange) and metal-ligand-metal (superexchange) interactions. The similar S covalencies for the MV model and Cu_A (Fig. 6A) indicate comparable thiolate S superexchange contributions to electronic coupling between the Cu atoms in both Cu_2S_2 centers. Therefore, the additional splitting of $\sim 7800\ cm^{-1}$ in Cu_A relative to the MV model reflects a direct Cu-Cu bonding interaction in oxidized Cu_A [99][15,16]. Further, Cu-Cu bonding also affects the energies of the the met-

[14] For Cu_A, we use the $\psi \rightarrow \psi^*$ label to denote the transition from the fully occupied Cu-Cu bonding MO to the half-occupied Cu-Cu antibonding MO, i.e., $\sigma \rightarrow \sigma^*$. For the MV model, the $\psi \rightarrow \psi^*$ transition is from the fully occupied π^* MO to the half-occupied π MO

[15] When compared to the literature on first-row transition metal dimers that have no ligand superexchange contributions to the σ-σ^* splittings [116], the analogous bond in Cu_A ($E_{\sigma-\sigma^*} \approx 7800\ cm^{-1}$) is not as strong. Further, a metal-metal bound would only be present in the oxidized site, since both the ψ and ψ^* orbitals are fully occupied in reduced Cu_A

[16] Our assignment of the 13,400 cm^{-1} transition to $\sigma \rightarrow \sigma^*$, which is based on the combination of absorption, CD, MCD, and resonance Raman enhancement data over a series of Cu_A centers [94, 112], is different from that of Thomson and co-workers [117] who assign the 9000 cm^{-1} band as $\sigma \rightarrow \sigma^*$. This alternative band assignment of $\sigma \rightarrow \sigma^*$ would still involve a 3400 cm^{-1} metal-metal contribution to $2H_{Cu\text{-}Cu}$, indicating that direct Cu-Cu bonding still contributes considerably (40%) to the total value of $2H_{Cu\text{-}Cu}$

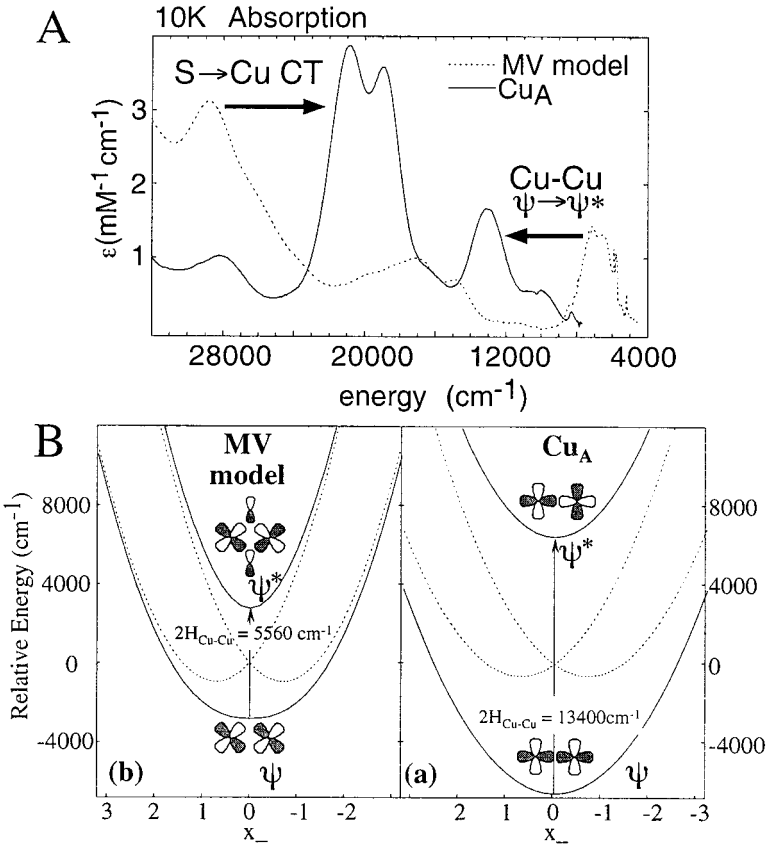

Fig. 7A,B Cu-Cu bonding and its effects in Cu_A. **A** The absorption spectrum shows an increase in $\psi \rightarrow \psi^*$ transition energy in Cu_A relative to the MV model. **B** Potential energy surfaces for Cu_A and the MV model showing the strong stabilization for valence delocalization in Cu_A due to metal-metal bonding

al-centered dimer orbitals such that different half-occupied redox active HOMOs are found for Cu_A and the MV model. The Cu-Cu bond in Cu_A raises the energy of the σ^*_u MO (Fig. 8, right) sufficiently that it becomes the HOMO (Fig. 9, right). Since the ~2.9 Å Cu-Cu distance in the MV model is too long for significant direct bonding to occur between coppers, the σ^*_u/σ_g splitting is due to thiolate superexchange that is only moderate in magnitude and results in a π_u HOMO in the MV model (Fig. 8 left, Fig. 9 left, vide infra).

The potential energy surfaces for a mixed valence copper dimer depend upon two factors: the electronic coupling between Cu ions ($H_{Cu\text{-}Cu}$), which favors valence delocalization as described above (solid lines in Fig. 7B), and vibronic trapping which stabilizes valence localization (by $1/4\ \Lambda^2/k_-$ in the x_- coordinate[17]) [118–120]. Vibronic trapping is associated with contraction of the ligand-metal bonds for Cu(II) relative to Cu(I). Equation 3 quantitatively describes this situation [118–120]:

$$E^{\pm} = \frac{1}{2}\left(\frac{\Lambda^2}{k_-}\right)x_-^2 \pm \left[\frac{1}{2}\left(\frac{\Lambda^2}{k_-}\right)^2 x_-^2 + H_{Cu-Cu}^2\right]^{1/2} \qquad (3)$$

In the absence of significant electronic coupling, a double-minima potential energy surface results (Fig. 7B, dotted) and gives a valence trapped dimer. When electronic coupling is significant relative to vibronic trapping, the result is a symmetric single-minimum potential associated with valence delocalization. Figure 7B compares the relative potential energy surfaces for Cu_A and the MV model (solid

[17] The (–) subscripts in Eq. 3 refer to the symmetry breaking nuclear coordinate comprised of the antisymmetric combination of monomeric (A,B) breathing motions, referred to as the Q_- in the PKS model [117], i.e., $Q_- = 2^{-1/2}(Q_A - Q_B)$, k_- is the force constant in this mode, $k_- = \pi^2 c^2 \mu_- \nu_-^2$, where ν_- and μ_- are the frequency and modal mass of the Q_- vibrational mode, respectively. Λ is the vibronic coupling parameter, where $\Lambda^2/k_- \approx k_-[n^{1/2}\Delta r_{redox}]^2$ in which n is the number of metal-ligand bond length changes and $\Delta\ r_{redox}$ is the difference in metal-ligand bond lengths between the oxidized and reduced structures. The quantity x_- is a dimensionless coordinate along the antisymmetric breathing mode, $x_- = Q_-/[\Lambda/k_-]$. Finally, $H_{Cu\text{-}Cu}$ is the electronic coupling matrix element regulating electron transfer between Cu ions in the dimer. See also [114, 115, 118–120]

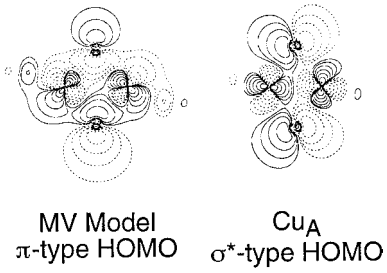

Fig. 8 The HOMOs of the MV model (*left*) and Cu_A (*right*)

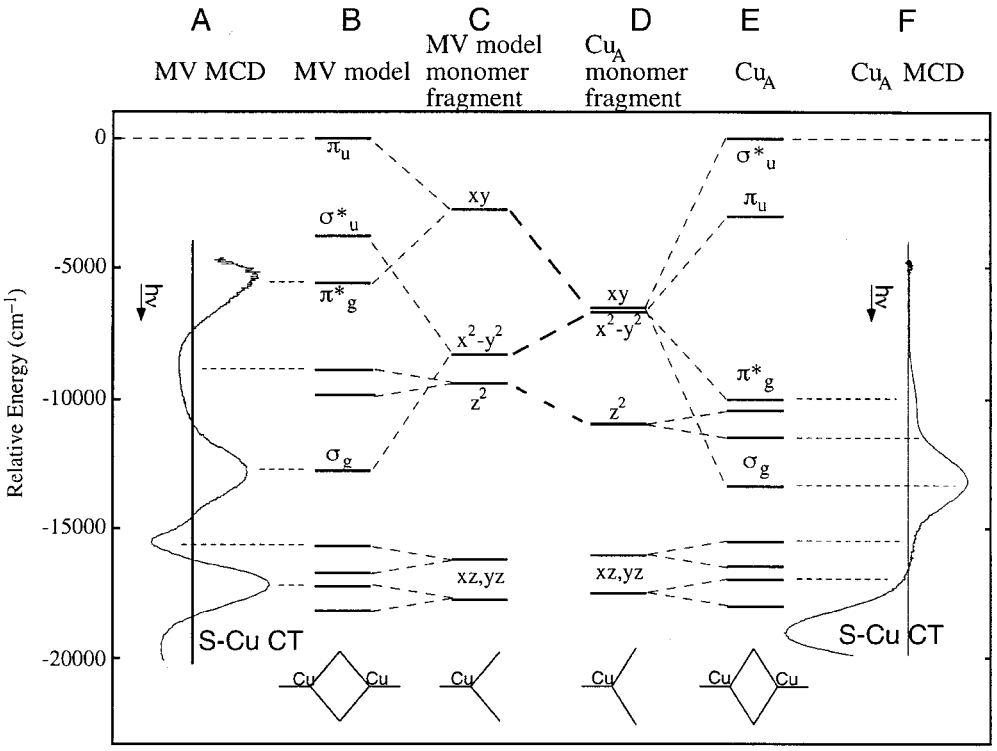

Fig. 9A–F Ligand field effects in Cu_A. Experimental correlation diagram relating the d orbital splitting patterns of Cu_A and the MV model. Columns **A**, **F** show MCD spectra of the metal-centered transitions of the MV model and Cu_A, from which energies of gerade levels in the dimer energy level diagram (columns **B**, **E**) are obtained. Columns **C** and **D** show the experimentally derived d-manifold energy pattern for a hypothetical monomer with the ligand field environment of the MV model and Cu_A. Note that the experimental energies were determined by a combination of absorption, CD, and MCD data. The π_u/σ^*_u splitting in the figure is from quantitative EPR analysis [100] and the $d z^2$ band at ~12,000 cm^{-1} is clear in the CD [94]. See footnote 18 for further discussion of u/g splitting values

lines, using experiment-based estimates for the terms in Eq. 3) relative to the trapped valence alternatives (dotted lines) [94]. The Cu-Cu bond in oxidized Cu_A significantly increases the magnitude of $H_{Cu\text{-}Cu}$ and consequently stabilizes the Cu_A core substantially more than the minimum required for valence delocalization. This extra stabilization enables the site to remain valence delocalized even in the asymmetric protein environment (with the different axial ligands in Fig. 1B). As described above, the fact that Cu_A remains valence delocalized reduces λ and likely places E° in a physiologically useful range, which both tend to maximize k_{ET}.

Protein structure influences in Cu_A

To understand the influence of the protein structure on the electronic structure of Cu_A, it is instructive to experimentally correlate its electronic structure to that of the MV model. In addition to Cu-Cu bonding effects (vide supra), the ligand field environments of Cu_A and the MV model also contribute to the respective electronic structures and thus the redox-active orbitals (i.e., HOMOs) [94]. As with the blue Cu centers, the ligand fields of Cu_A and the MV model are reflected in the experimental d→d transition energies which were determined by absorption, CD, and MCD spectroscopy (Fig. 9, columns A and F) [94, 117]. For these dimeric $Cu_2(SR)_2$ systems, the situation is complicated by the splitting of monomeric Cu d orbitals (Fig. 9, columns C and D) into gerade and ungerade dimer combinations due to metal-metal bonding and thiolate superexchange (Fig. 9, columns B and E). However, the experimental transition energies (from absorption, CD, and MCD spectra [94]) can be used[18] to extract the energies of the metal-based orbitals in hypothetical monomeric fragments, to estimate the ligand field environments of the Cu ions in Cu_A and the MV model, and to evaluate factors in the protein structure that may influence the electronic structure of oxidized Cu_A, including the formation of the Cu-Cu bond (Fig. 9).

The raised energy of the monomeric $d x^2-y^2$ orbital concomitant with the lowered energy of the monomeric $d xy$ orbital (Fig. 9, columns C and D) indicate that, relative to the MV model, the Cu ions in the Cu_2S_2 core of Cu_A are more trigonal [94]. In Cu_A, the $d z^2$ monomeric fragment orbital decreases in energy corresponding to a weakened axial interaction. The out-of-plane $d xz$ and $d yz$ orbital energies remain relatively constant between Cu_A and the MV model. The ligand field imposed by the protein, along with the increased dimer splitting of the σ^*_u/σ_g pair in Cu_A relative to the MV model (due to Cu-Cu bonding, vide supra), is responsible for the HOMO conversion from π_u in the MV model to σ^*_u in Cu_A (Figs. 8 and 9) [94].

[18] To construct Fig. 9 columns B and D, the following has been used. For Cu_A, quantitative EPR simulations [100] give the σ^*_u/π_u splitting as ~3500 cm^{-1}. For the MV model, the σ^*_u/σ_g splitting is set to 8000 cm^{-1}. For both Cu_A and the MV model, the energy splittings are of the out-of-plane ungerade orbital combinations (i.e., $(d z^2)_u$, $(d xz)_u$, and $(d yz)_u$) are set to 1000 cm^{-1}

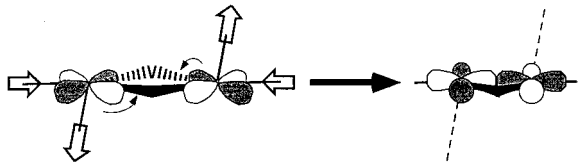

Fig. 10 Effects of the ligand field on the Cu_A center relative to the MV model. A weakened axial interaction on the Cu_A center is compensated by increased charge donation from equatorial N_{His}. These distortions rotate the HOMO from π_u to σ^*_u and introduce significant Cu-Cu bonding

This spectroscopically derived description of the ligand field is consistent with the crystallographically observed differences between Cu_A and the MV model: (1) a decrease of the Cu-Cu distance, where the $\angle$(S-Cu-S) increases from ~100° in the MV model [95] to ~116° in Cu_A [84–87]; and (2) a weakening of the axial ligand-Cu interaction. The weakened axial-Cu interaction is compensated by increases in charge donation from the in-plane N_{His} ligands, and thereby their influence on the electronic structure.

The protein environment of the Cu_A site could influence this ligand field in an analogous manner to that described above for the classic blue Cu centers. A weakened axial interaction [94] could be coupled to equatorial changes and the formation of a Cu-Cu bond. As depicted in Fig. 10, the Cu-N_{His} bonds likely contract to charge compensate for weakened axial ligands. Since the N_{His} atoms lie approximately on the Cu-Cu axis, the metal orbital lobes in the HOMO rotate to become more $d x^2-y^2$-like and are positioned favorably for σ overlap and Cu-Cu bonding which would then contract this bond. Thus, through weak axial and stronger equatorial interactions and the associated ligand field changes, the protein would provide an environment that is conducive to Cu-Cu bonding in the oxidized Cu_A center. This key feature can enhance the reactivity of the Cu_A center by allowing the valence to remain delocalized even in its asymmetric protein environment which benefits ET, as discussed above [94].

Summary

Several features of the electronic and geometric structures of these two classes of Cu ET proteins enhance their function in inter- and intra-protein ET. In blue Cu centers, experiments show the highly covalent nature of the Cu-S_{Cys} bond which enhances donor-acceptor electronic coupling, H_{AB}, for long-range ET [15, 36]. The ligand field of these sites, characterized by the long thioether and short thiolate interactions, decreases the reorganization energy, λ, by removing the possibility of a JT-induced distortion in the oxidized site [15, 41]. A decrease in the strength of the axial donor ligand interaction correlates with an increase in redox potential. As revealed by the series of perturbed spectra for blue Cu proteins with the same ligand set, the protein environment clearly plays a role in defining the geometric and electronic structure of the active site [67]. Also, a number of experimental results, including the existence of a green→blue point mutant involving the axial ligand [60], demonstrates that this ligand does indeed play a significant role in tuning the electronic structure. In the Cu_A center, the covalency of the thiolates could substantially enhance H_{AB} for ET from cytochrome *c* into the Cu_A center and contribute to ET to heme A [94]. The reorganization energy is minimized through the low frequency of the core bending mode of the binuclear center and the valence delocalized nature of the $Cu_2(S_{Cys})_2$ core [94]. Finally, by weakened axial interactions and associated equatorial ligand changes, the protein environment of the Cu_A center can provide a ligand field that is conducive to the formation of a Cu-Cu bond in the oxidized site. This is key to electronic delocalization in the low-symmetry protein environment which reduces λ and can adjust the potential such that $\Delta E^\circ+\lambda$ is small [94].

Acknowledgements We gratefully acknowledge the contributions of our collaborators cited in the original literature and financial support from the NSF (CHE-9528250) for this research. D.W.R. gratefully acknowledges a postdoctoral fellowship from the NIH (GM-18812).

References

1. Adman ET (1991) In: Anfinsen CB, Richards FM, Edsall JT, Eisenberg DS (eds) Advances in protein chemistry. Academic Press, San Diego, pp 145–198
2. Sykes AG (1991) Adv Inorg Chem 36:377–408
3. Messerschmidt A (1998) Struct Bonding 90:37–68
4. Baker EN (1994) In: King RB (ed) Encyclopedia of inorganic chemistry. Wiley, Chichester, pp 883–905
5. Solomon EI, Baldwin MJ, Lowery MD (1992) Chem Rev 92:521–542
6. Solomon EI, Lowery MD (1993) Science 259:1575–1581
7. Ferguson-Miller S, Babcock GT (1996) Chem Rev 96:2889–2907
8. Ramirez BE, Malmström BG, Winkler JR, Gray HB (1995) Proc Natl Acad Sci USA 92:11949–11951
9. Beinert H (1997) Eur J Biochem 245:521–532
10. Marcus RA, Sutin N (1985) Biochim Biophys Acta 811:265–322
11. Guss JM, Bartunik HD, Freeman HC (1992) Acta Crystallogr Sect B 48:790–811
12. Baker EN (1988) J Mol Biol 203:1071–1095
13. Nar H, Messerschmidt A, Huber R, van de Kamp M, Canters GW (1991) J Mol Biol 221:765–772
14. Lowery MD, Solomon EI (1992) Inorg Chim Acta 200:233–243
15. Solomon EI, Penfield KW, Gewirth AA, Lowery MD, Shadle SE, Guckert JA, LaCroix LB (1996) Inorg Chim Acta 243:67–78
16. Malmström BG, Vänngård T (1960) J Mol Biol 2:118–124
17. Bates CA, Moore WS, Standley KJ, Stevens KWH (1962) Proc Phys Soc 79:73
18. Sharnoff M (1965) J Chem Phys 42:3383
19. Brill AS, Bryce GR (1968) J Chem Phys 48:4398–4404
20. Roberts JE, Brown TG, Hoffman BM, Peisach J (1980) J Am Chem Soc 102:825

21. Shadle SE, Penner-Hahn JE, Schugar HJ, Hedman B, Hodgson KO, Solomon EI (1993) J Am Chem Soc 115:767–776
22. Hughey JL IV, Fawcett TG, Rudich SM, Lalancette RA, Potenza JA, Schugar HJ (1979) J Am Chem Soc 101:2617–2623
23. George SJ, Lowery MD, Solomon EI, Cramer SP (1993) J Am Chem Soc 115:2968–2969
24. Penfield KW, Gay RR, Himmelwright RS, Eickman NC, Norris VA, Freeman HC, Solomon EI (1981) J Am Chem Soc 103:4382–4388
25. Slater JC (1974) Quantum theory of molecules and solids. McGraw-Hill, New York
26. Johnson KH, Norman JG Jr, Connolly JWD (1973) In: Herman F, McLean AD, Nesbet RK (eds) Computational methods for large molecules and localized states in solids. Plenum, New York, pp 161–201
27. Penfield KW, Gewirth AA, Solomon EI (1985) J Am Chem Soc 107:4519–4529
28. Gewirth AA, Solomon EI (1988) J Am Chem Soc 110:3811–3819
29. LaCroix LB, Shadle SE, Wang YN, Averill BA, Hedman B, Hodgson KO, Solomon EI (1996) J Am Chem Soc 118:7755–7768
30. Werst MM, Davoust CE, Hoffman BM (1991) J Am Chem Soc 113:1533–1538
31. Larsson S, Broo A, Sjölin L (1995) J Phys Chem 99:4860–4865
32. Pierloot K, De Kerpel JOA, Ryde U, Roos BO (1997) J Am Chem Soc 119:218–226
33. Messerschmidt A, Ladenstein R, Huber R, Bolognesi M, Petruzzelli R, Rossi A, Finazzi-Agró A (1992) J Mol Biol 224:179–205
34. Adman ET, Godden JW, Turley S (1995) J Biol Chem 270:27458–27474
35. Kyritsis P, Lundberg LG, Nordling M, Vänngård T, Young S, Tomkinson NP, Sykes AG (1991) J Chem Soc Chem Commun 1441–1442
36. Lowery MD, Guckert JA, Gebhard MS, Solomon EI (1993) J Am Chem Soc 115:3012–3013
37. Beratan DN, Betts JN, Onuchic JN (1991) Science 252:1285–1288
38. Lin JY, Jones P, Guckert J, Solomon EI (1991) J Am Chem Soc 113:8312–8326
39. Lin JY, Jones PM, Lowery MD, Gay RR, Cohen SL, Solomon EI (1992) Inorg Chem 31:686–695
40. Lin JY, May JA, Didziulis SV, Solomon EI (1992) J Am Chem Soc 114:4718–4727
41. Guckert JA, Lowery MD, Solomon EI (1995) J Am Chem Soc 117:2817–2844
42. Holm RH, Kennepohl P, Solomon EI (1996) Chem Rev 96:2239–2314
43. Botuyan MV, Toy-Palmer A, Chung J, Blake RC II, Beroza P, Case DA, Dyson JH (1996) J Mol Biol 263:752–767
44. Stephens PJ, Jollie DR, Warshel A (1996) Chem Rev 96:2491–2513
45. Zhou H-X (1997) JBIC 2:109–113
46. Bertini I, Gori-Savellini G, Luchinat C (1997) JBIC 2:114–118
47. Mauk AG, More GR (1997) JBIC 2:119–125
48. Gunner MR, Alexov E, Torres E, Lipovaca S (1997) JBIC 2:126–134
49. Náray-Szabó G (1997) JBIC 2:135–138
50. Armstrong FA (1997) JBIC 2:139–142
51. Warshel A, Papazyan A, Muegge I (1997) JBIC 2:143–152
52. Xu F, Berka RM, Wahleithner JA, Nelson BA, Shuster JR, Brown SH, Palmer AE, Solomon EI (1998) Biochem J 334:63–70
53. Yaver DS, Xu F, Golightly EJ, Brown KM, Brown SH, Rey MW, Schneider P, Halkier T, Mondorf K, Dalboge H (1996) Appl Environ Microbiol 62:834–841
54. Xu F, Palmer AE, Yaver DS, Berka RM, Gambetta GA, Brown SH, Solomon EI (1999) J Biol Chem 274:12372–12375
55. Pascher T, Karlsson G, Nordling M, Malmström BG, Vänngård T (1993) FEBS Lett 272:289–296
56. Kroes SJ, Hoitink CWG, Andrew CR, Ai J, Sanders-Loehr J, Messerschmidt A, Hagen WR, Canters GW (1996) Eur J Biochem 240:342–351
57. Romero A, Hoitink CWG, Nar H, Huber R, Messerschmidt A, Canters GW (1993) J Mol Biol 229:1007–1021
58. Nersissian AM, Immoos C, Hill MG, Hart PJ, Williams G, Herrmann RG, Valentine JS (1998) Protein Sci 7:1915–1929
59. Kataoka K, Nakai M, Yamaguchi K, Suzuki S (1999) J Inorg Biochem 74:188
60. Olesen K, Veselov A, Zhao Y, Wang Y, Danner B, Scholes CP, Shapleigh JP (1998) Biochemistry 37:6086–6094
61. Williams RJP (1995) Eur J Biochem 234:363–381
62. James BR, Williams RJP (1961) J Chem Soc 2007–2019
63. Guss JM, Harrowell PR, Murata M, Norris VA, Freeman HC (1986) J Mol Biol 192:361–387
64. Ballhausen CJ (1962) Introduction to ligand field theory. McGraw-Hill, New York, pp 62–69
65. Malmström BG (1994) Eur J Biochem 223:711–718
66. Stoffels ALE, Haanstra WG, Driessen WL, Reedijk J (1990) Angew Chem Int Ed Engl 29:1419
67. LaCroix LB, Randall DW, Nersissian AM, Hoitink CWG, Canters GW, Valentine JS, Solomon EI (1998) J Am Chem Soc 120:9621–9631
68. Lu Y, LaCroix LB, Lowery MD, Solomon EI, Bender CJ, Peisach J, Roe JA, Gralla EB, Valentine JS (1993) J Am Chem Soc 115:5907–5918
69. Aikazyan VT, Nalbandyan RM (1975) FEBS Lett 55:272–274
70. Sakurai T, Okamoto H, Kawahara K, Nakahara A (1982) FEBS Lett 147:220–224
71. Han J, Loehr TM, Lu Y, Valentine JS, Averill BA, Sanders-Loehr J (1993) J Am Chem Soc 115:4256–4263
72. Andrew CR, Sanders-Loehr J (1996) Acc Chem Res 29:365–372
73. Guss JM, Merritt EA, Phizackerley RP, Freeman HC (1996) J Mol Biol 259:686–705
74. Han J, Adman ET, Beppu T, Codd R, Freeman HC, Huq L, Loehr TM, Sanders-Loehr J (1991) Biochemistry 30:10904–10913
75. Ryde U, Olsson MHM, Pierloot K, Roos BO (1996) J Mol Biol 261:586–596
76. Pierloot K, De Kerpel JOA, Ryde U, Olsson MHM, Roos BO (1998) J Am Chem Soc 120:13156–13166
77. Olsson MHM, Ryde U, Roos BO, Pierloot K (1998) JBIC 3:109–125
78. De Kerpel JOA, Pierloot K, Ryde U, Roos BO (1998) J Phys Chem B 102:4638–4647
79. Kroneck PMH, Antholine WE, Riester J, Zumft WG (1988) FEBS Lett 242:70–74
80. Kroneck PMH, Antholine WA, Riester J, Zumft WG (1989) FEBS Lett 248:212–213
81. Malmström BG (1998) JBIC 3:339–343
82. Regan JJ, Ramirez BE, Winkler JR, Gray HB, Malmström BG (1998) J Bioenerg Biomembr 30:35–39
83. Babcock GT, Wikström M (1992) Nature 356:301–307
84. Iwata S, Ostermeier C, Ludwig B, Michel H (1995) Nature 376:660–669
85. Ostermeier C, Harrenga A, Ermler U, Michel H (1997) Proc Natl Acad Sci USA 94:10547–10553
86. Tsukihara T, Aoyama H, Yamashita E, Tomizaki T, Yamaguchi H, Shinzawaitoh K, Nakashima R, Yaono R, Yoshikawa S (1995) Science 269:1069–1074
87. Tsukihara T, Aoyama H, Yamashita E, Tomizaki T, Yamaguchi H, Shinzawaitoh K, Nakashima R, Yaono R, Yoshikawa S (1996) Science 272:1136–1144
88. Williams PA, Blackburn NJ, Sanders D, Bellamym H, Stura EA, Fee JA, McRee DE (1999) Nat Struct Biol 6:509–516

89. Robinson H, Ang MC, Gao Y-G, Hay MT, Lu Y, Wang AH-J (1999) Biochemistry 38 : 5677–5683
90. Blackburn NJ, de Vries S, Barr ME, Houser RP, Tolman WB, Sanders D, Fee JA (1997) J Am Chem Soc 119 : 6135–6143
91. Blackburn NJ, Barr ME, Woodruff WH, van der Oost J, de Vries S (1994) Biochemistry 33 : 10401–10407
92. Wilkström M (1998) J Bioenerg Biomembr 30 : 3–5
93. Andrew CR, Fraczkiewicz R, Czernuszewicz RS, Lappalainen P, Saraste M, Sanders-Loehr J (1996) J Am Chem Soc 118 : 10436–10445
94. Gamelin DR, Randall DW, Hay MT, Houser RP, Mulder TC, Canters GW, de Vries S, Tolman WB, Lu Y, Solomon EI (1998) J Am Chem Soc 120 : 5246–5263
95. Houser RP, Young VG Jr, Tolman WB (1996) J Am Chem Soc 118 : 2101–2102
96. Harding C, McKee V, Nelson J (1991) J Am Chem Soc 113 : 9684–9685
97. Barr ME, Smith PH, Antholine WE, Spencer B (1993) J Chem Soc Chem Commun 1649–1652
98. LeCloux DD, Davydov R, Lippard SJ (1998) J Am Chem Soc 120 : 6810–6811
99. Williams KR, Gamelin DR, LaCroix LB, Houser RP, Tolman WB, Mulder TC, de Vries S, Hedman B, Hodgson KO, Solomon EI (1997) J Am Chem Soc 119 : 613–614
100. Neese F, Zumft WG, Antholine WE, Kroneck PMH (1996) J Am Chem Soc 118 : 8692–8699
101. Neese F, Kappl R, Zumft WG, Hüttermann J, Kroneck PMH (1998) JBIC 3 : 53–67
102. Witt H, Malatesta F, Nicoletti F, Brunori M, Ludwig B (1998) J Biol Chem 273 : 5132–5136
103. Reister J, Kroneck PMH, Zumft WG (1989) Eur J Biochem 178 : 751–762
104. Chan SI, Li PM (1990) Biochemistry 29 : 1–12
105. Lappalainen P, Aasa R, Malmström BG, Saraste M (1993) J Biol Chem 268 : 26416–26421
106. Morgan JE, Wilkström M (1991) Biochemistry 30 : 948–958
107. Fraga E, Webb MA, Loppnow GR (1996) J Phys Chem 100 : 3278–3287
108. Zhou Z, Kahn SUM (1989) J Phys Chem 93 : 5292–5295
109. Bu Y, Ding Y, He F, Jiang L, Song X (1997) Int J Quantum Chem 61 : 117–126
110. Larsson S, Kallebring B, Wittung P, Malmström BG (1995) Proc Natl Acad Sci USA 92 : 7167–7171
111. Bominaar EL, Achim C, Borshch SA, Girerd JJ, Münck E (1997) Inorg Chem 36 : 3689–3701
112. Wallace-Williams SE, James CA, de Vries S, Saraste M, Lappalainen P, van der Oost J, Fabian M, Palmer G, Woodruff WH (1996) J Am Chem Soc 118 : 3986–3987
113. Hupp JT, Zhang XL (1995) J Phys Chem 99 : 853–855
114. Gamelin DR, Bominaar EL, Mathonière C, Kirk ML, Wieghardt K, Girerd J-J, Solomon EI (1996) Inorg Chem 35 : 4323–4335
115. Gamelin DR, Bominaar EL, Kirk ML, Wieghardt K, Solomon EI (1996) J Am Chem Soc 118 : 8085–8097
116. Abrahamson HB, Frazier CC, Ginley DS, Gray HB, Lilienthal J, Tyler DR, Wrighton MS (1977) Inorg Chem 16 : 1554–1556
117. Farrar JA, Neese F, Lappalainen P, Kroneck PMH, Saraste M, Zumft WG, Thomson AJ (1996) J Am Chem Soc 118 : 11501–11514
118. Piepho SB, Krausz ER, Schatz PN (1978) J Am Chem Soc 100 : 2996–3005
119. Schatz PN (1999) In: Solomon EI, Lever ABP (eds) Inorganic electronic structure and spectroscopy, vol 2. Wiley, New York, pp 175–226
120. Blondin G, Girerd J-J (1990) Chem Rev 90 : 1359–1379